Available online at www.sciencedirect.com
SCIENCE DIRECT®
Applied Catalysis A: General 249 (2003) 53–67
APPLIED CATALYSIS A: GENERAL
www.elsevier.com/locate/apcata

Liquid phase hydrogenation of cinnamaldehyde on Cu-based catalysts

Alberto J. Marchi*, Diego A. Gordo, Andrés F. Trasarti, Carlos R. Apesteguía

Instituto de Investigaciones en Catálisis y Petroquímica (INCAPE), CONICET-UNL, Santiago del Estero 2654, (3000) Santa Fe, Argentina

Received 19 September 2002; received in revised form 20 February 2003; accepted 23 February 2003

Abstract

The liquid phase hydrogenation of cinnamaldehyde was studied at 393 K and 10 bar on Cu-based catalysts containing about 12 wt.% of copper. Cu/SiO_2 was prepared by incipient wetness impregnation while Cu–Al, Cu–Zn–Al, and Cu–Ni(Co)–Zn–Al catalysts were obtained by coprecipitation at constant pH. Cinnamaldehyde was initially hydrogenated to cinnamyl alcohol and hydrocinnamaldehyde, and these products consecutively yielded hydrocinnamyl alcohol. Hydrogenation kinetic constants were determined by modeling catalytic data and using a pseudohomogeneous kinetic network. The reaction occurred via two different pathways depending on the composition and surface properties of the catalyst. On Cu/SiO_2 and binary Cu–Al samples, cinnamaldehyde hydrogenation proceeded via a monofunctional pathway on metallic copper that produced predominantly hydrocinnamaldehyde. Ternary Cu–Zn–Al and quaternary Cu–Ni(Co)–Zn catalysts were about one order of magnitude more active than Cu/SiO_2 for cinnamaldehyde conversion and produced predominantly cinnamyl alcohol. The general composition formula of reduced Cu–Zn–Al and Cu–Ni(Co)–Zn–Al catalysts was $Cu^0_{0.5}\cdot[MO]_{0.5}\cdot ZnAl_2O_4$, where M is Zn, Co, or Ni. These catalysts contained the Cu^0 particles highly dispersed in a super-stoichiometric zinc aluminate spinel and in close interaction with M^{2+} cations. The presence of M^{2+} cations provided a new reaction pathway for adsorbing and hydrogenating cinnamaldehyde in addition to the metal copper active sites. Cinnamaldehyde interacts linearly via the C=O group with M^{2+} sites and is selectively hydrogenated to unsaturated alcohol by atomic hydrogen activated in neighboring Cu^0 sites. Formation of surface Cu^0–M^{2+} sites was, therefore, crucial to efficiently catalyze the cinnamyl alcohol formation from cinnamaldehyde via a dual-site reaction pathway.

Keywords: Cinnamaldehyde hydrogenation; Selective hydrogenation; Aldehydes (α,β-unsaturated); Copper-based catalysts; Spinel-like catalysts

1. Introduction

Hydrogenation of α,β-unsaturated aldehydes to the corresponding allyl alcohols is of great importance in Fine Chemistry because the reaction products are widely used as flavors and perfumes, as well as intermediates for the synthesis of valuable organic molecules [1]. The reaction is also studied from a fundamental point of view because it poses an interesting problem of chemo- and regioselectivity. In fact, α,β-unsaturated aldehydes may be transformed to unsaturated alcohols via the selective hydrogenation of C=O bonds or to saturated aldehydes by

* Corresponding author.
E-mail address: amarchi@fiqus.unl.edu.ar (A.J. Marchi).

0926-860X/$ – see front matter © 2003 Elsevier Science B.V. All rights reserved.
doi:10.1016/S0926-860X(03)00199-6

exclusively hydrogenating C=C groups. Both types of products are then consecutively hydrogenated to yield the corresponding saturated alcohols. Furthermore, additional formation of unwanted products may also occur by unsaturated alcohol hydrogenolysis or by decarbonylation or condensation of unsaturated aldehydes [2,3]. Desirable catalyst properties are, therefore, the ability to selectively hydrogenate the C=O bond and the aptitude for avoiding formation of unwanted byproducts via secondary reactions.

Catalysts based on noble metals, such as Pt, Pd, Ru, or Rh, have been widely studied for hydrogenation of α,β-unsaturated aldehydes [4–20]. However, noble metals hydrogenate the C=C bond faster than the C=O group [21,22], and addition of promoters is often required for improving the selectivity to unsaturated alcohols [4–7,16–20]. Authors have followed different approaches to modify the intrinsic catalytic properties of noble metals: (1) addition of a second metal to form bimetallic compounds, such as Pt–Fe, Pt–Ru, Pt–Co, or Pd–Fe [4–7]; (2) use of zeolites and reducible supports, like TiO_2 [8–13]; (3) use of special low-temperature reduction methods [14,15]; (4) addition of metal cations, such as Sn^{n+} [16–20]. The observed enhancement in the selectivity towards C=O hydrogenation was explained on the basis of different factors, such as the metal electron density increase by either formation of bimetallic compounds [4–7] or interaction with the support [8–11], geometric effects [12,13], and C=O bond polarization by its interaction with cationic sites [16–20].

The use of non-noble metals for selectively hydrogenating α,β-unsaturated aldehydes has also been reported in literature. Nickel and copper have shown interesting characteristics of chemo-, regio-, and stereoselectivity for hydrogenation reactions [23–27], but do not exhibit a high selectivity to form unsaturated alcohols from α,β-unsaturated aldehydes [24–29]. Attempts for improving the intrinsic catalytic properties of copper and nickel include formation of bimetallic Ni–Cu particles [26] and the interaction between metal and support, as in the case of Cu/Cr_2O_3 [27]. Poisoning of copper catalysts by chlorine or sulfur compounds also increases the selectivity to unsaturated alcohol, but at the expense of important activity decay [28,29].

Lately, increasing research efforts have been devoted to develop novel catalysts for selectively hydrogenating the carbonyl group. Potential interesting catalytic materials are multimetallic non-stoichiometric spinel-like oxides prepared by decomposition at low temperatures of coprecipitated precursors [30–32]. After activation in H_2, these solids usually contain the metal particles highly dispersed in a super-stoichiometric spinel matrix, in close interaction with dipositive cations. As it has been reported [16–20], formation of surface metal-cation sites may selectively promote the C=O bond hydrogenation of α,β-unsaturated aldehydes.

In this work, we prepared by coprecipitation a set of catalysts containing very small Cu^0 particles highly dispersed in a super-stoichiometric zinc aluminate spinel phase. The general catalyst formula, in a spinel-like basis, was $Cu^0_{0.5}\cdot[MO]_{0.5}\cdot ZnAl_2O_4$, where M^{2+} is Zn^{2+}, Co^{2+}, or Ni^{2+}. These catalysts were tested in the liquid phase hydrogenation of cinnamaldehyde (3-phenyl-2-propenal) and compared with the catalytic performance of a monofunctional Cu/SiO_2 catalyst prepared by impregnation. Our objective was to explore the possibility of dramatically improving the intrinsic catalytic properties of copper to hydrogenate the C=O group by generating a high density of dual Cu^0–M^{2+} active sites. Results will show that the initial formation rate of cinnamyl alcohol on $Cu^0_{0.5}\cdot[MO]_{0.5}\cdot ZnAl_2O_4$ catalysts is about two orders of magnitude higher than on Cu/SiO_2, thereby increasing the initial selectivity towards cinnamyl alcohol by a factor between 10 and 20. We explain these results by considering that formation of dual metal-cation sites provides a new reaction pathway to achieve the selective allyl alcohol synthesis. A pseudohomogeneous kinetic model that accounts for both monofunctional hydrogenation on Cu and dual-site reaction on Cu^0–M^{2+} sites is used for interpreting experimental data.

2. Experimental

2.1. Catalyst preparation

Cu/SiO_2 (SiO_2, Grace 62, 99.7%) sample was prepared by incipient wetness impregnation by dropwise addition of an aqueous solution of $Cu(NO_3)_2\cdot 3H_2O$ with a copper concentration of 0.6 M. The impregnated sample was first dried at 353 K

overnight and then decomposed in N_2 at 673 K for 6 h.

Hydrated precursors of binary Cu–Al, ternary Cu–Zn–Al, and quaternary Cu–Ni(Co)–Al mixed oxides were prepared by coprecipitation as described elsewhere [33–35]. An acidic solution of the metal nitrates was contacted with an aqueous solution of K_2CO_3 at a constant pH of 7. The two solutions were simultaneously added dropwise to 400 ml of distilled water kept at 333 K in a stirred batch reactor. The resulting precipitates were aged for 2 h at 333 K in their mother liquor and then filtered, washed thoroughly with deionized water at 333 K, and finally dried at 353 K overnight. Dried precipitates were decomposed overnight in nitrogen at 773 K in order to obtain the corresponding mixed oxides.

2.2. Catalyst characterization

The solid structure and crystal size in the catalytic precursors before and after decomposition were determined by X-ray diffraction (XRD) methods, in the range of $2\theta = 10$–80°, using a Shimadzu XD-D1 diffractometer and Ni-filtered Cu Kα radiation ($\lambda = 1.540$ Å). Surface area (S_g), pore volume (V_p), and pore distribution of mixed oxides were determined by adsorption–desorption of N_2 at 77 K in a Micromeritics Accusorb 2100 sorptometer, by using the BET equation for surface area and the BJH method for pore distribution calculations. Elemental compositions were measured by atomic absorption spectroscopy (AAS), using a Perkin Elmer 3110 spectrometer.

The temperature programmed reduction (TPR) experiments were performed in a 5% H_2/N_2 gaseous mixture at 30 $cm^3\,min^{-1}$ STP. The sample size was 50–100 mg. Samples were heated at 10 K min^{-1} within the temperature range of 293–1023 K. Since water is formed during sample reduction, the gas exiting from the reactor was passed through a cold trap before entering the thermal conductivity detector.

Hydrogen chemisorption was measured by volumetric adsorption experiments at room temperature in a conventional vacuum apparatus. Catalysts were reduced in H_2 at 473 K for 1 h and then outgassed at the same temperature under a vacuum of 10^{-7} bar. After cooling to room temperature, a first isotherm was drawn for measuring the total H_2 uptake (HC). Then, and after 1 h of evacuation at room temperature, a second isotherm was drawn to determine the amount of weakly adsorbed H_2. The amount of strongly chemisorbed H_2 (HC_i) was calculated as the difference between total and weakly adsorbed H_2. The pressure range of isotherms was 0–0.15 bar and extrapolation to zero pressure was used as a measure of the gas uptake on copper.

2.3. Catalytic testing

The liquid phase hydrogenation of cinnamaldehyde (CAL) was studied in a Parr 4563 reactor at 393 K and 10 bar, and using isopropanol as solvent. The autoclave was loaded with 150 ml of isopropanol, 10 ml of cinnamaldehyde, and 1 g of catalyst (particles of 0.35–0.42 mm diameter). Prior to catalytic tests, samples were activated ex situ in flowing hydrogen (30 ml min^{-1}) at 473 K for 1 h. The reaction system was heated until 393 K at 2 K min^{-1} and the pressure was then rapidly increased to 10 bar with H_2.

The concentrations of unreacted CAL and of the reaction products were followed during the reaction by ex situ gas chromatography using a Varian Star 3400 CX chromatograph equipped with flame ionization detector, temperature programmer, and a 30 m Carbowax Amine capillary column. Samples from the reaction system were taken by using a loop under pressure in order to avoid flushing. Data were collected every 15–30 min for 250–500 min. The reaction products were hydrocinnamaldehyde (3-phenylpropanal), cinnamyl alcohol (3-phenyl-2-propen-1-ol), and hydrocinnamyl alcohol (3-phenyl-1-propanol). Cinnamaldehyde conversion (X_{CAL}, mol of CAL reacted/mol of CAL fed) was calculated as $X_{CAL} = (C^0_{CAL} - C_{CAL})/C^0_{CAL}$, where C^0_{CAL} is the initial concentration of cinnamaldehyde and C_{CAL} is the cinnamaldehyde concentration at reaction time t. Selectivities (S_i, mol of product i/mol of CAL reacted) were calculated as $S_i\,(\%) = 100C_i/\sum C_i$ where C_i is the concentration of reaction product i. Product yields (η_i, mol of product i/mol of CAL fed) were calculated as $\eta_i = S_i X_{CAL}$. It was verified that diffusional restrictions do not corrupt measured initial reaction rates by carrying out experiments with different catalyst particle sizes and varying the stirrer speed.

Table 1
Chemical composition, XRD characterization, and physical properties of the samples used in this work

Catalyst	Elemental analysis (wt.%)[a]				XRD analysis			Physical properties[b]		
	Cu	Ni or Co	Zn	Al	Hydrated precursor	Mixed oxide crystallite size (Å)		S_g ($m^2\,g^{-1}$)	V_p ($cm^3\,g^{-1}$)	d_p[c] (nm)
						Spinel	CuO			
Cu/SiO_2	12.5	–	–	–	$Cu(NO_3)_2$	–	275	218	0.78	7.4
Cu–Al	12.8	–	–	45.2	Amorphous	–	–	230	0.24	7.4
Cu–Zn–Al	12.7	–	37.3	20.5	Hydrotalcite	47	–	221	0.46	12.4
Cu–Ni–Zn–Al	12.3	11.3	24.8	21.0	Hydrotalcite	<40	–	235	0.40	9.2
Cu–Co–Zn–Al	12.2	11.5	25.0	20.8	Hydrotalcite	110	–	210	0.38	9.4

[a] Bulk composition of mixed oxides measured by AAS.
[b] Values measured for mixed oxides.
[c] Calculated pore diameter.

3. Results and discussion

3.1. Catalyst characterization

3.1.1. Chemical and phase compositions of the samples

The crystalline phases of hydrated precursors and mixed oxides were determined by XRD technique (Table 1). No crystalline phases were detected for coprecipitated Cu–Al sample. XRD patterns showed a single crystalline phase with hydrotalcite structure for Cu–Zn–Al and Cu–Ni(Co)–Zn–Al coprecipitated samples. Diffraction patterns are consistent with the proposed hydrotalcite structure, consisting of layered double hydroxides with brucite-like layers and $[(\sum Me^{2+})_{1-x}Al_x(OH)_2]^{x+}(CO_3)_{x/2}{}^{2-}\cdot mH_2O$ composition, where Me is Cu, Zn, Ni, or Co. The stoichiometric hydrotalcite structure, $(\sum Me^{2+})_6Al_2(OH)_{16}CO_3\cdot mH_2O$, is reached when x is 0.25 (ASTM 14-191).

Thermal decomposition of hydroxycarbonate precursors led to the formation of mixed oxides of high surface area and large pore volume (Table 1). The S_g values of mixed oxides (210–235 $m^2\,g^{-1}$) were significantly higher than those of corresponding hydrotalcite precursors; it appears that the removal of CO_2 and H_2O during decomposition leads to the formation of significant porosity. The intimate contact between Me and Al cations in the hydrotalcite structure is preserved during decomposition and leads to the formation of well-mixed Me_yAlO_x oxides [30,31,36]. The specific surface area of Cu/SiO_2 sample was similar to those of mixed oxides prepared by coprecipitation (Table 1).

XRD patterns of the hydrated precursors after decomposition in N_2 at 773 K are shown in Fig. 1. Cu/SiO_2 exhibited a single crystalline phase of CuO (ASTM 5-0661) with large crystallite size. Binary Cu–Al was a quasi-amorphous sample. Ternary Cu–Zn–Al and quaternary Cu–Ni(Co)–Zn–Al samples showed diffraction patterns consistent with the presence of spinel-like phases (ASTM 5-0669 and 10-458). No segregation of CuO or ZnO crystalline phases were detected in Cu–Zn–Al mixed oxide, thereby indicating that both cations are highly

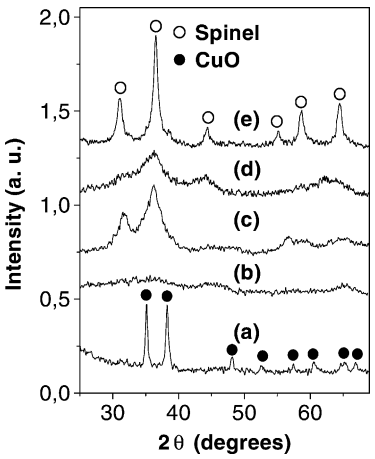

Fig. 1. XRD patterns of samples obtained by decomposition of hydrated precursors in N_2 at 773 K: Cu/SiO_2 (a), Cu–Al (b), Cu–Zn–Al (c), Cu–Ni–Zn–Al (d), and Cu–Co–Zn–Al (e).

dispersed in the spinel-like matrix. Similarly, crystalline Cu(Co,Ni)O_x binary phases were not detected in quaternary Cu–Ni(Co)–Zn–Al samples.

Mixed oxides compositions were measured by AAS and are shown in Table 1. Elemental analysis of decomposed coprecipitated precursors gave Al/(Al + Me) atomic ratios very similar to those present in the precursor solution, consistent with complete precipitation of Me and Al salts during synthesis. The potassium content was below 0.1 wt.%, which confirms that K^+ ions were effectively removed by filtration and washing of the precipitated precursors. In all the samples, Cu loading was between 12 and 13 wt.%. In ternary and quaternary mixed oxides, the $(\sum Me^{2+})$/Al ratio was about 1. In Cu–Ni(Co)–Zn–Al samples the [Zn + Ni(Co)]/Al and Zn/Al ratios were 0.75 and 0.5, respectively. This composition corresponds to $[CuO]_{0.5}\cdot[Ni(Co)O]_{0.5}\cdot ZnAl_2O_4$ spinel-like formulations [31,32,34]. The Zn/Al ratio for ternary Cu–Zn–Al samples was 0.75, which in a spinel-like basis gives rise to a $[CuO]_{0.5}\cdot[ZnO]_{0.5}\cdot ZnAl_2O_4$ formula.

3.1.2. Reducibility and surface properties

TPR profiles of the hydrated precursors after decomposition in N_2 at 773 K are shown in Fig. 2. Cu/SiO_2 exhibits a broad peak with a maximum at 610 K (Table 2) resulting from the reduction of CuO [33,37]. Similarly, TPR traces of Cu–Al and Cu–Zn–Al samples show only single CuO reduction peaks, but the peak maxima (590 and 570 K, respectively) are shifted to lower temperatures compared to Cu/SiO_2. No evidences of $CuAl_2O_4$ formation were detected in Cu–Al and Cu–Zn–Al samples, which are consistent with XRD characterization. Bulk $CuAl_2O_4$ spinel is thermodynamically unstable below 873 K [38], but formation of $CuAl_2O_4$ surface spinels containing the Cu^{2+} ions in a distorted octahedral geometry has been observed at much lower temperatures [39]. The TPR trace of Cu–Co–Zn–Al sample exhibits a low-temperature peak at 490 K corresponding to

Table 2
Catalyst characterization: TPR and H_2 chemisorption results

Catalyst	TPR: CuO reduction peak		H_2 uptake	
	T_m[a] (K)	Δ_w[b] (K)	HC[c] ($cm^3\,g^{-1}$)	HC_i/HC[d]
Cu/SiO_2	610	85	0.322	0.44
Cu–Al	582	75	0.936	0.53
Cu–Zn–Al	575	43	1.507	0.36
Cu–Ni–Zn–Al	550	20	1.733	0.37
Cu–Co–Zn–Al	490	17	1.802	0.39

[a] Temperature peak maximum.
[b] Peak width.
[c] HC: total chemisorbed hydrogen.
[d] HC_i: strongly chemisorbed hydrogen.

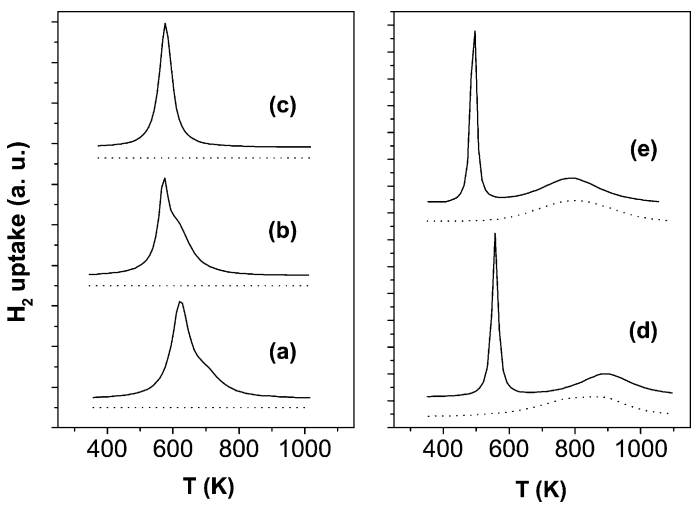

Fig. 2. TPR profiles of Cu-based samples following treatments in N_2 at 773 K (full lines) and in H_2 at 473 K (dotted lines): Cu/SiO_2 (a), Cu–Al (b), Cu–Zn–Al (c), Cu–Ni–Zn–Al (d), and Cu–Co–Zn–Al (e).

CuO reduction and a broad H_2 consumption band at higher temperatures, between 750 and 1000 K, which is attributed to the reduction of Co^{2+} ions highly dispersed in a $ZnAl_2O_4$ spinel [31,34]. Because formation of $ZnAl_2O_4$ spinel is thermodynamically favored compared to normal $CoAl_2O_4$ spinel [31,34], it is expected that the spinel-like phase formed at low temperatures in Cu–Co–Zn–Al samples is essentially $ZnAl_2O_4$. Thus, Zn^{2+} and Co^{2+}ions would occupy the tetrahedral sites and octahedral sites, respectively, of the non-stoichiometric spinel phase [31,34]. No evidences of the presence of bulk CoO or Co_3O_4 phases were found in Cu–Co–Zn–Al sample. CoO reduces at about 650 K while Co_3O_4 spinels typically reduce in a two peak TPR profile between 550 and 700 K [40,41]. In previous papers dealing with characterization of ternary Cu–Co–Al mixed oxides, we observed that the use of inert atmospheres for decomposing hydrated Cu–Co–Al precursors prevents the formation of Co_3O_4 [35,41]. Finally, the TPR profile of Cu–Ni–Zn–Al sample shows a low-temperature peak at 550 K resulting from CuO reduction and a broad band between 650 and 950 K, which corresponds to the reduction of Ni^{2+} ions located in octahedral holes of the $ZnAl_2O_4$ spinel [32], as explained above for Cu–Co–Zn–Al sample.

Table 2 shows the values of temperature maximum (T_m) and the peak width (Δ_w) for the CuO reduction peaks obtained from TPR curves. In a previous work [36] on the kinetics and mechanism of CuO reduction in Cu–Zn–Al mixed oxides, we found that both T_m and Δ_w increase with increasing CuO particle size (L_{CuO}). We interpreted these results by modeling the CuO reduction data in terms of the unreacted shrinking core model assuming chemical control at the boundary interface [42]. The unreacted shrinking core model considers that reduction of non-porous particles occurs at the metal/metal oxide interface and is characterized by constantly decreasing reaction rates as the substrate particle is consumed in the course of the reaction. Computer calculations using this model predict that, in agreement with experimental data, both T_m and Δ_w should increase by increasing L_{CuO} [43]. Table 2 shows that T_m and Δ_w decrease in the order Cu/SiO_2 > Cu/Al > Cu–Zn–Al > Cu–Ni(Co)–Zn–Al and we can reasonably expect, therefore, that L_{CuO} decreases following the same trend.

Additional TPR experiments were performed to obtain insight on the metal reduction degree of the catalysts loaded in the reactor for carrying out catalytic tests. All the samples were reduced in a flow of pure H_2 at 473 K for 1 h prior to the catalytic measurements. In order to ascertain the effect of this reduction treatment on the final oxidation state of the metal species, we treated initially the samples in the TPR unit in H_2 at 473 K for 1 h and then we performed a standard TPR experiment. Results are shown in Fig. 2. TPR profiles of Cu/SiO_2, Cu–Al, and Cu–Zn–Al samples do not reveal any H_2 consumption, thereby suggesting that CuO is completely reduced to Cu^0 by the pretreatment in pure H_2 at 473 K. In the case of quaternary Cu–Ni(Co)–Zn–Al samples, and by comparing with TPR profiles of unreduced Cu–Ni(Co)–Zn–Al samples, it is observed in Fig. 2 that after reduction in H_2 at 473 K the low-temperature peak resulting from CuO reduction disappears but the high-temperature consumption bands corresponding to the reduction of Co^{2+} or Ni^{2+} ions are practically not modified. Quantification of hydrogen consumption confirmed that the H_2 amount consumed in the high-temperature band was the same for unreduced and pre-reduced quaternary samples.

The metallic fraction of the catalysts was characterized by hydrogen chemisorption at room temperature. Prior to volumetric adsorption experiments, samples were reduced in pure H_2 at 473 K for 1 h. As noted above, in all the samples this treatment reduces completely CuO to metallic Cu but does not reduce Co^{2+}(Ni^{2+}) ions in quaternary Cu–Ni(Co)–Zn–Al samples. Hydrogen chemisorption data would be essentially related then to the reduced copper fraction of the catalysts. Results are shown in Table 2. The total chemisorbed hydrogen (HC, $cm^3\,g^{-1}$ Cu) increases in the order Cu/SiO_2 < Cu/Al < Cu–Zn–Al < Cu–Ni(Co)–Zn–Al, but the HC_i/HC ratio, where HC_i is the strongly chemisorbed hydrogen, is about 0.35–0.45 for all the samples. The HC increase trend reflects the increase of the metallic Cu dispersion from Cu/SiO_2 to quaternary Cu–Ni(Co)–Zn–Al samples. This result is in complete agreement with the TPR characterization data showed previously. On the other hand, the fact that the HC_i/HC ratio is similar for all the samples reveals that the fraction of strongly chemisorbed H_2 does not depend significantly on either the Cu particle size or the copper interaction with the support.

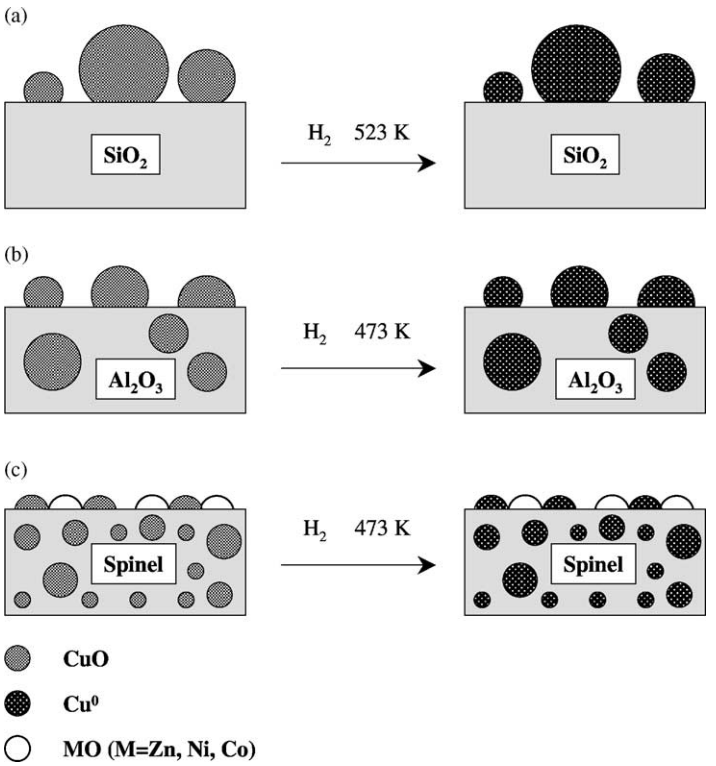

Scheme 1. Simplified representation of surface and bulk species on unreduced and reduced Cu-based catalyst used in this work.

3.1.3. Sample structure

Characterization results showed that all the samples present similar textural properties, i.e. specific surface area, pore volume, and pore radius, but different structural and surface properties. Unreduced Cu/SiO_2 contains large CuO crystallites with a tenorite-like structure. After reduction with H_2, large Cu^0 particles presenting very low interaction with the SiO_2 support are formed (Scheme 1a). Cu–Zn–Al and Cu–Ni(Co)–Zn–Al samples contain the Cu(Co,Ni)O single oxides very well dispersed in a non-stoichiometric zinc aluminate-like phase. Treatment with hydrogen at 473 K transforms completely CuO to metallic copper, but does not reduce Co^{2+} and Ni^{2+} cations. Reduced Cu–Ni(Co)–Zn–Al catalysts contain then very small Cu^0 particles that are highly interdispersed in a non-stoichiometric spinel phase (Scheme 1c). The high dispersion of small Cu^0 crystallites in the spinel matrix favors the generation of surface Cu–M^{2+} dual sites, where M = Zn, Ni, and Co [44]. An intermediate situation regarding both metal crystallite size and metal–support interaction should be expected for binary Cu–Al sample (Scheme 1b).

3.2. Cinnamaldehyde hydrogenation

3.2.1. Cinnamaldehyde conversion and reaction pathways on Cu-based catalysts

Hydrogenation reactions of cinnamaldehyde on metal-based catalysts proceed via parallel and consecutive reaction pathways that involve hydrogenation of C=O and C=C groups. Cinnamaldehyde hydrogenation on our Cu-based catalysts formed essentially cinnamyl alcohol (COL), hydrocinnamaldehyde (SAL), and hydrocinnamyl alcohol (SOL). The evolution of CAL conversion with reaction time for all the catalysts is shown in Fig. 3. CAL conversion rates on ternary Cu–Zn–Al and quaternary Cu–Ni(Co)–Zn–Al catalysts were significantly higher than on Cu–Al and Cu/SiO_2. After 5 h reaction, CAL was totally consumed on Cu–Zn–Al and Cu–Ni(Co)–Zn–Al catalysts, but X_{CAL} was only about 0.4 and 0.6 on Cu/SiO_2

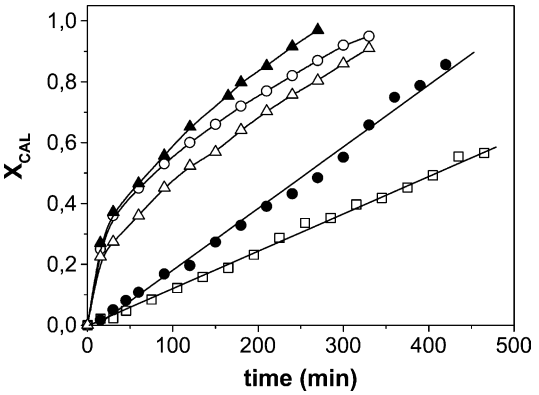

Fig. 3. Cinnamaldehyde conversion as a function of time [393 K, 10 bar, 1 g catalyst]: Cu/SiO_2 (□), Cu–Al (●), Cu–Zn–Al (○), Cu–Ni–Zn–Al (▲), Cu–Co–Zn–Al (△).

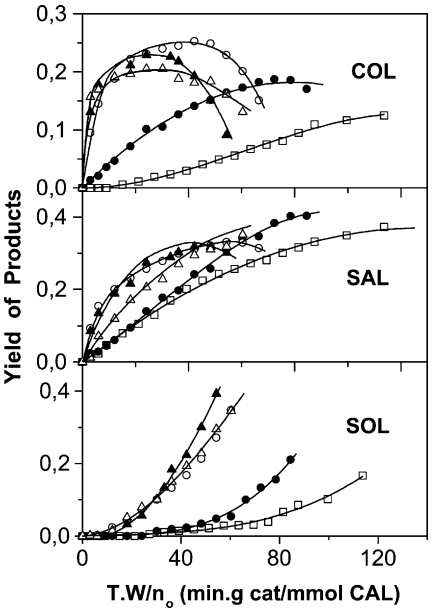

Fig. 4. Product distribution for cinnamaldehyde hydrogenation reactions on Cu-based catalysts. Product yield (η_i) as a function of parameter Wt/n_T^0 [393 K, 10 bar, 1 g catalyst]: Cu/SiO_2 (□), Cu–Al (●), Cu–Zn–Al (○), Cu–Ni–Zn–Al (▲), Cu–Co–Zn–Al (△).

and Cu–Al, respectively. Initial CAL conversion rates (r_0, g mol h^{-1} g^{-1} catalyst) were calculated by polynomial extrapolation to zero time and are shown in Table 3. The r_0 values obtained on Cu–Zn–Al and Cu–Ni(Co)–Zn–Al catalysts are about one order of magnitude higher compared to those calculated on Cu–Al and Cu/SiO_2. Fig. 3 also shows that X_{CAL} increases linearly with time on Cu–Al and Cu/SiO_2 samples, but not on Cu–Zn–Al and Cu–Ni(Co)–Zn–Al, thereby suggesting that cinnamaldehyde is transformed following different reaction rate expressions.

Product yields are shown in Fig. 4 for all the catalysts as a function of Wt/n_T^0, where W is the catalyst weight and t the reaction time. The local slope for each product in Fig. 4 gives its rate of formation at a specific value of reactant conversion and contact time. The non-zero initial slope for COL and SAL shows that these products are formed directly from cinnamaldehyde. Both, COL and SAL reach maximum yields as they convert to SOL in consecutive hydrogenations, but maximum values are reached faster for COL than for SAL, particularly on Cu–Zn–Al and Cu–Ni(Co)–Zn–Al catalysts. The zero initial slope of SOL yield curve is consistent with its formation via the secondary hydrogenation of primary COL and SAL products. SOL formation rates are clearly higher on

Table 3
Catalytic results on Cu-based catalysts for cinnamaldehyde hydrogenation in liquid phase

Catalyst	r_0 (g mol min^{-1} g^{-1})	Selectivity (%)					
		X_{CAL} = 30%			X_{CAL} = 60%		
		COL	SAL	SOL	COL	SAL	SOL
Cu/SiO_2	5.8×10^{-4}	10.7	79.6	9.7	21.7	59.5	18.8
Cu–Al	1.7×10^{-3}	38.6	60.1	1.3	19.6	52.7	27.7
Cu–Zn–Al	8.3×10^{-3}	47.5	42.1	10.4	38.1	42.3	19.6
Cu–Ni–Zn–Al	8.9×10^{-3}	48.5	31.5	20.0	36.4	40.4	23.2
Cu–Co–Zn–Al	7.5×10^{-3}	52.9	33.5	13.6	36.0	36.1	27.9

$T = 393$ K; $P_{H_2} = 10$ bar; $W = 1$ g.

Cu–Zn–Al and Cu–Ni(Co)–Zn–Al than on Cu–Al and Cu/SiO_2 catalysts.

The product selectivities at two fixed CAL conversions for all the samples are shown in Table 3. At $X_{CAL} = 30\%$, Cu/SiO_2 and Cu–Al samples form predominantly SAL, thereby showing that they selectively catalyze the hydrogenation of C=C bonds. In contrast, COL was the most abundant product formed on Cu–Zn–Al and Cu–Ni(Co)–Zn–Al catalysts at the same conversion level, reaching S_{COL} values of about 50%. As expected, at higher CAL conversion the selectivity toward SOL, which is the terminal product in the reaction network, increases on all the catalysts. Except for Cu/SiO_2, the selectivity to SAL was higher than to COL at $X_{CAL} = 60\%$ because COL is converted more rapidly to SOL (Fig. 4). On Cu/SiO_2, the COL selectivity increased from 10.7% at $X_{CAL} = 30\%$ to 21.7% at $X_{CAL} = 60\%$, probably reflecting the induction period observed for COL formation on this catalyst (Fig. 4).

Finally, a couple of catalytic tests were carried out on unreduced Cu–Zn(Co,Ni)–Al samples (i.e. the sample pretreatment with H_2 at 473 K was avoided) to investigate the effect of reduction on catalytic activity. It was found that cinnamaldehyde conversion was negligible after 6 h reaction, thereby indicating that the presence of metallic copper is required for hydrogenating the reactant. Only the metal Cu atoms are, therefore, able in our catalysts to generate active hydrogen atoms by adsorbing and dissociating the hydrogen molecule.

3.2.2. Reaction kinetics modeling

In order to determine the hydrogenation kinetic constant values, we performed a kinetic study by modeling catalytic data using a pseudohomogeneus model. The observed effects of residence time on product yields (Fig. 4) and previous literature reports [3,45] lead us to propose the reaction network described in Fig. 5. Reactions 7 and 8 are considered to be negligible on our Cu-based catalysts because we did not detect formation of any COL hydrogenolysis or CAL decarbonylation products. The direct hydrogenation of CAL to SOL (reaction 6, Fig. 5) is also not included for modeling since our results in Fig. 4 clearly show that SOL is not a primary product of the CAL conversion reactions. Thus, the kinetics of CAL conversion reactions is represented by the following differential equations system, which includes the CAL conversion rate and the formation rates of COL, SAL, and SOL:

$$r_{CAL} = -\frac{dC_{CAL}}{dt} = k_1(C_{CAL})^{\mu} + k_2(C_{CAL})^{\nu} \quad (1)$$

$$r_{COL} = \frac{dC_{COL}}{dt} = k_1(C_{CAL})^{\mu} - k_3C_{COL} - k_5C_{COL} \quad (2)$$

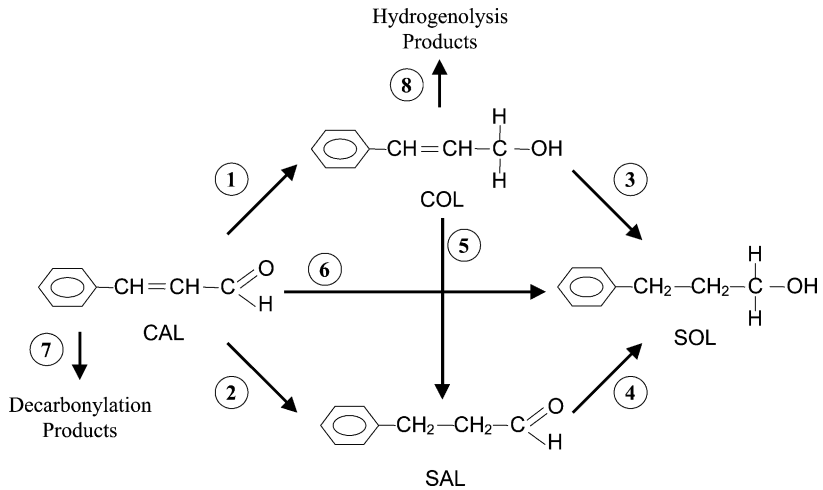

Fig. 5. Reaction network for cinnamaldeyde hydrogenation reactions.

$$r_{SAL} = \frac{dC_{SAL}}{dt} = k_2(C_{CAL})^{\nu} - k_4 C_{SAL} + k_5 C_{COL} \quad (3)$$

$$r_{SOL} = \frac{dC_{SOL}}{dt} = k_3 C_{COL} + k_4 C_{SAL} \quad (4)$$

μ and ν are the reactions orders with respect to CAL for CAL hydrogenation to COL and SAL, respectively. Reaction orders equal to one are assumed for both hydrogenation of COL and SAL into SOL, and isomerization of COL into SAL, on the basis of data obtained on Cu-based catalysts by other authors [46,47].

Differential equations were integrated analytically or numerically depending on reaction orders and the equation system considered. Numerical integration was performed by using the Runge–Kutta–Merson algorithm. The model parameter estimation was performed by non-linear regression, using a Levenberg–Marquardt algorithm which minimizes the objective function $Q = \sum(C_{i,j} - C^*_{i,j})^2$, where C and C^* are the experimental and calculated concentrations, respectively, i the chemical compound, and j the reaction time. The best agreement between experimental data and model predictions was obtained by assuming that the kinetic constant for CAL isomerization to COL is negligible ($k_5 = 0$) for all the catalysts and that reactions orders μ and ν are zero on Cu/SiO_2 and Cu–Al samples, and 2 and 1, respectively, on both Cu–Zn–Al and Cu–Zn–Ni(Co)–Al catalysts. Figs. 6 and 7 compare the time evolution of product concentrations for Cu–Al and Cu–Zn–Al catalysts. Similar goodness-of-fit was obtained with the other catalysts when concentrations were plotted as a function of time. The values of reactions orders μ and ν, kinetic constants k_i, and k_1/k_2 ratios obtained at 393 K are given in Table 4.

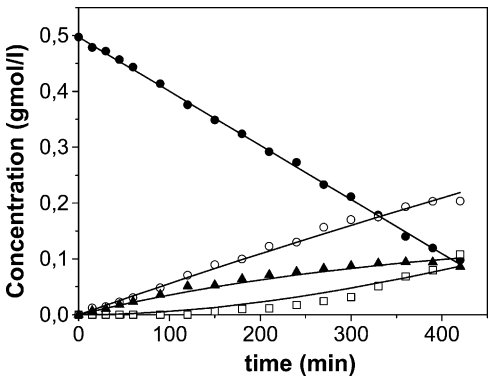

Fig. 6. Reactant and product concentrations for cinnamaldehyde hydrogenation on Cu–Al catalyst [393 K, 10 bar, 1 g catalyst]. Points, experimental results; solid lines, model predictions: CAL (●), COL (▲), SAL (○), and SOL (□).

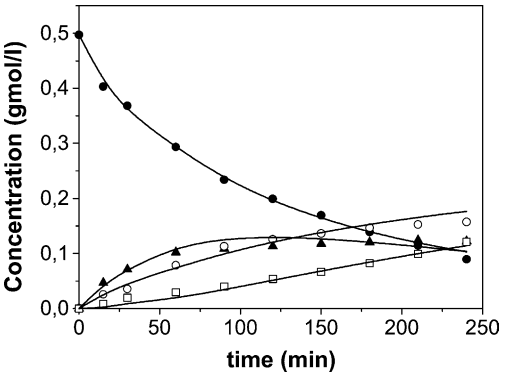

Fig. 7. Reactant and product concentrations for cinnamaldehyde hydrogenation on Cu–Zn–Al catalyst [393 K, 10 bar, 1 g catalyst]. Points, experimental results; solid lines, model predictions: CAL (●), COL (▲), SAL (○), and SOL (□).

Rate constants k_1 and k_2 are much higher for Cu–Zn–Al and Cu–Ni(Co)–Zn–Al catalysts than for Cu–Al and Cu/SiO_2, which are consistent with the experimental values of initial CAL conversion rates shown in Table 3. On the other hand, the k_1/k_2 ratio on Cu–(Ni,Co)–Zn–Al samples is about 20 times higher than on Cu/SiO_2 and reflects similar qualitative difference obtained on the same catalysts for initial COL/SAL selectivity ratios (see Table 3, selectivities at $X_{CAL} = 30\%$). Finally, rate constants k_3 and k_4, which represent the SOL formation from COL and SAL, respectively, are similar on Cu–Zn–Al and Cu–Ni(Co)–Zn–Al catalysts. These catalysts show higher ($k_3 + k_4$) values compared to Cu–Al and Cu/SiO_2 samples and are more active than for producing SOL. Binary Cu–Al sample forms SOL essentially from COL; in contrast, Cu/SiO_2 produces SOL by selective hydrogenation of SAL.

In summary, catalytic results of liquid phase cinnamaldehyde hydrogenation show that the Cu-based catalysts used in this work may be divided in two groups following their catalytic performances: (a) Cu/SiO_2 and Cu–Al present a low activity to transform CAL and hydrogenate preferentially the C=C bond exhibiting high selectivities to SAL. Reaction

Table 4
Kinetic parameters of cynnamaldehyde hydrogenation on Cu-based catalysts determined by modeling experimental data

Catalyst	Order		Kinetic constants[a]				k_1/k_2
	μ	ν	k_1[b]	k_2[b]	k_3 ($\mathrm{min^{-1}\,g^{-1}}$)	k_4 ($\mathrm{min^{-1}\,g^{-1}}$)	
Cu/SiO_2	0	0	$1.0 \times 10^{-4} \pm 1.1 \times 10^{-5}$	$5.0 \times 10^{-4} \pm 1.6 \times 10^{-5}$	0	$1.5 \times 10^{-3} \pm 2.4 \times 10^{-4}$	0.2
Cu–Al	0	0	$4.4 \times 10^{-4} \pm 1.8 \times 10^{-5}$	$5.6 \times 10^{-4} \pm 1.2 \times 10^{-5}$	$3.2 \times 10^{-3} \pm 5.0 \times 10^{-4}$	0	0.8
Cu–Zn–Al	2	1	$1.1 \times 10^{-2} \pm 9.5 \times 10^{-4}$	$4.4 \times 10^{-3} \pm 3.0 \times 10^{-4}$	$2.1 \times 10^{-3} \pm 7.2 \times 10^{-4}$	$3.3 \times 10^{-3} \pm 1.7 \times 10^{-3}$	2.5
Cu–Ni–Zn–Al	2	1	$1.8 \times 10^{-2} \pm 3.5 \times 10^{-3}$	$5.0 \times 10^{-3} \pm 9.2 \times 10^{-4}$	$5.4 \times 10^{-3} \pm 2.0 \times 10^{-3}$	$2.7 \times 10^{-3} \pm 1.7 \times 10^{-3}$	3.6
Cu–Co–Zn–Al	2	1	$1.2 \times 10^{-2} \pm 1.5 \times 10^{-3}$	$3.1 \times 10^{-3} \pm 4.2 \times 10^{-4}$	$6.0 \times 10^{-3} \pm 1.4 \times 10^{-3}$	$4.3 \times 10^{-4} \pm 2.3 \times 10^{-4}$	3.9

$T = 393\,\mathrm{K}$; $P_{H_2} = 10\,\mathrm{bar}$, $W = 1\,\mathrm{g}$.

[a] Intervals calculated with a 95% of confidence.

[b] $\mu = \nu = 0$, $[k_1] = [k_2] = \mathrm{g\,mol\,min^{-1}\,l^{-1}\,g^{-1}}$; $\mu = 2$, $[k_1] = \mathrm{l\,g\,mol\,min^{-1}\,g^{-1}}$; $\nu = 1$, $[k_2] = \mathrm{min^{-1}\,g^{-1}}$.

orders with respect to CAL for CAL conversion to SAL and COL are zero on both catalysts; (b) Cu–Zn–Al and Cu–Ni(Co)–Zn–Al catalysts show high activity for converting CAL and produce mainly COL by selectively hydrogenating the C=O group of the CAL molecule. Reaction orders with respect to CAL are 2 and 1 for CAL conversion to COL and SAL, respectively.

3.3. Sample composition and catalytic performance

Catalytic results strongly suggest that cinnamaldehyde hydrogenation on Cu-based catalysts occurs via different reaction mechanisms depending on the composition and surface properties of the catalyst (see Table 4). Cu/SiO_2 sample, which contains the largest mean Cu^0 crystallite size of the catalyst set, showed low activity for converting CAL and was less selective towards the formation of COL. Because SiO_2 is an inert support and the interaction between the large Cu^0 crystallites and the support is weak, CAL hydrogenation on Cu/SiO_2 would occur via a monofunctional mechanism on metallic copper. Reaction order in CAL is zero on Cu/SiO_2, probably because the surface of large metal copper crystallites is rapidly saturated by the adsorption of CAL molecules [45]. CAL adsorption on metal copper particles is expected to occur via π_{CC} and/or d_i–π adsorption modes [48], being both of them influenced by the repulsive forces existing between copper d orbitals and the phenyl group of cinnamaldehyde (Scheme 2a). Initially, CAL is selectively hydrogenated to SAL because copper surface saturation by the reactant seems to inhibit hydrogenation of C=O group. Formation of COL is detected after an induction period, probably because formation of clean metal surface patches during reaction that allow the CAL molecules to interact with the copper surface via d_i–σ_{CO} or π_{CO} adsorption modes (Scheme 2a). Nevertheless, the SAL formation rate remains significantly higher than that of COL during the entire catalytic test.

The catalytic behavior of binary Cu–Al catalyst was qualitatively similar to that of Cu/SiO_2. In fact, on binary Cu–Al sample the reaction order with respect to CAL is zero and CAL is predominantly hydrogenated to SAL. However, CAL conversion rate is higher on Cu–Al catalyst than on Cu/SiO_2 and no induction periods are observed for COL formation.

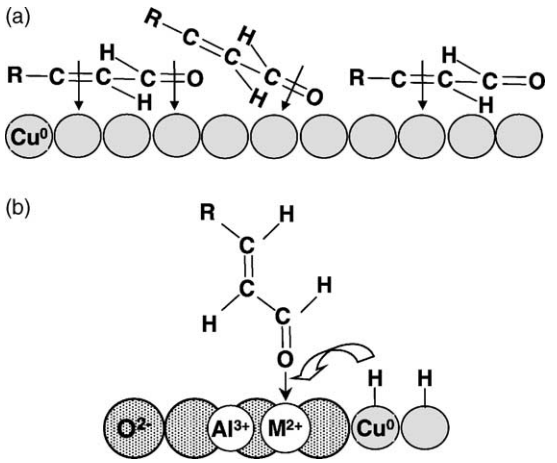

Scheme 2. Adsorption modes of cinnamaldehyde molecule over Cu-based catalysts used in this work.

Both differences are explained by taking into account that the Cu^0 crystallite size is significantly lower on Cu–Al than on Cu/SiO_2, thereby increasing the number of metallic surface active sites. Alumina is a better support for dispersing copper as compared to silica, but does not provide itself active centers for CAL hydrogenation; the reaction on Cu–Al catalyst proceeds then via a monofunctional metallic pathway.

Ternary Cu–Zn–Al catalyst contains very small Cu^0 particles that are highly dispersed in a super-stoichiometric zinc aluminate phase; the catalyst formula, in a spinel-like basis, is $Cu^0_{0.5}\cdot[ZnO]_{0.5}\cdot ZnAl_2O_4$. The high dispersion of small Cu^0 crystallites and the super-stoichiometric Zn concentration in the spinel matrix favor the interaction between Cu^0 particles and Zn^{2+} cationic sites. Cu–Zn–Al catalyst is about one order of magnitude more active than Cu/SiO_2, and hydrogenates preferentially the C=O groups of the CAL molecule forming predominantly COL. These catalytic results may be explained by considering that the presence of Zn^{2+} cations provides new surface sites for adsorbing and hydrogenating CAL in addition to the metal copper active sites. Cationic Zn^{2+} sites are able to adsorb CAL molecules via an on-top adsorption (Scheme 2b) which favors the activation of C=O group [48]. Copper is very active for adsorbing H_2 dissociatively and may furnish by spillover activated atomic hydrogen to selectively hydrogenate the C=O group in CAL molecules adsorbed on Zn^{2+}

sites. A close interaction between Cu^0 and Zn^{2+} active sites is required, therefore, to catalyze efficiently this dual-site reaction pathway leading from CAL to COL. CAL hydrogenation to COL via a dual-site mechanism is consistent with the second order reaction in CAL found on Cu–Zn–Al catalyst. Cinnamaldehyde is preferentially hydrogenated to COL on Cu–Zn–Al catalyst, but the CAL conversion rate to SAL on this catalyst is also significantly higher than on Cu/SiO_2. This late result essentially reflects the higher copper dispersion existing in Cu–Zn–Al catalyst compared to Cu/SiO_2.

Reduced Cu–Ni(Co)–Zn catalyst compositions are $Cu_{0.5}{\cdot}[(Ni,Co)O]_{0.5}{\cdot}ZnAl_2O_4$, in a spinel-like formulation. Compared to Cu–Zn–Al composition, it is observed that the Zn^{2+} in excess to stoichiometric $ZnAl_2O_4$ spinel in Cu–Zn–Al sample has been replaced by Co^{2+} or Ni^{2+} cations. Thus, in Cu–Ni(Co)–Zn samples the small Cu^0 crystallites are in interaction not only with Zn^{2+}, but also with $Ni(Co)^{2+}$ cations placed in octahedral holes of the non-stoichiometric spinel matrix. The activity and selectivities for CAL conversion reactions on Cu–Ni(Co)–Zn catalysts are very similar to those found on ternary Cu–Zn–Al catalyst. This shows that the COL formation rate is essentially increased on Cu–Ni(Co)–Zn–Al catalysts compared to Cu/SiO_2 or binary Cu–Al samples because of the formation of surface Cu^0–M^{2+} dual sites, irrespective of the nature of M^{2+} cations (Co, Ni, Zn).

Finally, it is worth noticing that a direct comparison between our Cu-based samples and noble metal-based catalysts regarding catalytic activity and selectivity is not straightforward. In fact, papers dealing with the liquid phase hydrogenation of cinnamaldehyde on Pt-, Ru-, and Rh-based catalysts have been carried out at different pressure, temperature, and catalyst/reactant ratios than those used in this work. Besides, noble metal loadings are substantially lower than the copper content in our catalysts and it is expected then that the catalyst structure as well as the interaction of metal–support were different when comparing both kind of catalysts. Nevertheless, an initial comparison can be done by considering noble metal-based catalysts of negligible metal–support interaction and containing Pt(Rh,Ru)–$M^{\delta+}$ dual sites of similar nature to those detected in our Cu-based catalysts.

Regarding monometallic Pt(Rh,Ru,Pd)/C catalysts, Giroir-Fendler et al. [12] found that the selectivity to cinnamyl alcohol follows the order Pt > Ru > Rh > Pd. The selectivity to cinnamyl alcohol at 333 K and 25% conversion was 33% on Pt/C and 5% on Ru/C. Lashdaf et al. [49] studied the liquid phase hydrogenation of cinnamaldehyde on $Ru(Pd)/Al_2O_3$ catalysts at 333 K and 10 bar hydrogen pressure. The selectivity to cinnamyl alcohol was between 11 and 24% at 65% conversion on Pd/Al_2O_3 and between 20 and 30% at 30% conversion on Ru/Al_2O_3. These values are similar to those obtained on our Cu–Al catalyst at 393 K (see Table 3).

In the case of supported Pt(Rh,Ru)–$M^{\delta+}$ binary catalysts, several researchers [6,16,18,50] have proposed that the addition of Fe and Sn to Pt- and Ru-based catalysts generates surface acid Lewis-type sites that can activate the C=O functional group of cinnamaldehyde. Then, hydrogen dissociatively adsorbed on contiguous metal surface atoms can hydrogenate the activated C=O terminal group. For instance, it has been reported [6,50] that the addition of Fe to monometallic Pt/C catalysts in a Pt/Fe ratio of 0.2 increases the selectivity to cinnamyl alcohol up to about 70–85%. For Fe/Pt ratios higher than 0.2, both the activity and selectivity into cinnamyl alcohol decrease, probably because the active metal phase becomes covered with Fe. Monometallic Pt/Nylon 66 catalyst is inactive for hydrogenating the C=O group of cinnamaldehyde, but the addition of 25% Sn produces cinnamyl alcohol with a selectivity of 75% [16]. Similar trends have been observed for Ru–Sn/C catalysts: selectivities to cinnamyl alcohol as high as 90% at 90% conversion were found for 30% Sn [18]. In all cases, the cinnamyl alcohol selectivity increase was attributed to the ability of surface $Fe^{\delta+}$($Sn^{\delta+}$) electrophilic sites for activating the C=O group of cinnamaldehyde via the lone electron pair of oxygen. Results of this work show that the intrinsic activity of copper for the formation of cinnamyl alcohol is increased by two orders of magnitude when copper interacts with a spinel-like matrix and forms Cu–M^{2+} sites. But concomitantly the hydrogenation rate for the C=C bond of cinnamaldehyde also increases (although to a lesser degree) and the selectivities to cinnamyl alcohol reported here on our Cu catalysts are lower as compared to those mentioned previously on Pt–Sn(Fe) and Ru–Sn catalysts. However, the density of surface Cu–M^{2+} can be probably increased by optimizing the catalyst composition, particularly Cu content, and would cause a further

improvement in the catalyst ability for selectively hydrogenating the C=O group of α,β-unsaturated aldehydes.

4. Conclusions

Cinnamaldehyde hydrogenation on Cu/SiO_2 and binary Cu–Al samples occurs via a monofunctional pathway on metallic copper. The cinnamaldehyde adsorption mode on copper favors hydrogenation of the C=C group in the cinnamaldehyde molecule forming mainly the unsaturated aldehyde. Increasing the Cu dispersion increases cinnamaldehyde conversion rate, but does not modify significantly the catalyst selectivity. Alumina is a better support for dispersing copper as compared to silica, but does not provide itself active centers for cinnamaldehyde hydrogenation.

Ternary Cu–Zn–Al and quaternary Cu–Ni(Co)–Zn catalysts are about one order of magnitude more active than Cu/SiO_2 and produce predominantly cinnamyl alcohol. These catalysts contain very small Cu^0 particles highly dispersed in a super-stoichiometric zinc aluminate spinel phase; their general formula, in a spinel-like basis, is $Cu^0_{0.5}\cdot[MO]_{0.5}\cdot ZnAl_2O_4$, where M is Zn, Co, or Ni. The high dispersion of Cu^0 crystallites and the super-stoichiometric M concentration in the spinel matrix favor the interaction between Cu^0 particles and M^{2+} cationic sites. The presence of surface Cu^0–M^{2+} sites in $Cu^0_{0.5}\cdot[MO]_{0.5}\cdot ZnAl_2O_4$ catalysts provides a new reaction pathway for selectively hydrogenating cinnamaldehyde to cinnamyl alcohol. M^{2+} sites adsorb cinnamaldehyde linearly via an η_1 on-top adsorption, thereby favoring the activation of C=O group. Copper adsorbs H_2 dissociatively and furnishes by spillover the activated atomic hydrogen necessary to hydrogenate the C=O group in cinnamaldehyde molecules adsorbed on M^{2+} sites. A close interaction between Cu^0 and M^{2+} active sites is, therefore, crucial to efficiently catalyze the cinnamyl alcohol formation from cinnamaldehyde via a dual-site reaction pathway.

Acknowledgements

We thank the Universidad Nacional del Litoral (UNL), Consejo Nacional de Investigaciones Científicas y Técnicas (CONICET), and Agencia Nacional de Promoción Científica y Tecnológica (ANPCyT), Argentina, for the financial support of this work. We are grateful to E. Rincón for chemisorption measurements.

References

[1] K. Bauer, D. Garbe, "Ullmann's Encyclopedia", vol. A11, 3rd ed., VCH, New York, 1988, p. 141.
[2] M. Englisch, A. Jentys, J.A. Lercher, J. Catal. 166 (1997) 25.
[3] R.L. Augustine, L. Meng, in: Proceedings of the 16th Conference on Catalysis of Organic Reactions, The Organic Reactions Catalysis Society, Atlanta, Georgia, April 1996.
[4] M. Englisch, V.S. Ranade, J.A. Lercher, J. Mol. Catal. A: Chemical 121 (1997) 69.
[5] P. Fouilloux, Heterogeneous catalysis and fine chemicals, in: M. Guisnet, J. Barrault, C. Bouchoule, D. Duprez, C. Montassier, G. Pérot (Eds.), Proceedings of the International Symposium, Poitiers, 15–17 March 1988, Stud. Surf. Sci. Catal., vol. 41, Elsevier, Amsterdam, 1988, p. 123.
[6] D. Goupil, P. Fouilloux, R. Maurel, React. Kinet. Catal. Lett. 35 (1/2) (1987) 185.
[7] W. Yu, Y. Wang, H. Liu, W. Zheng, J. Mol. Catal. A: Chemical 112 (1996) 105.
[8] F. Coloma, A. Sepúlveda-Escribano, F. Rodríguez-Reinoso, Appl. Catal. A: General 123 (1995) L1.
[9] F. Coloma, A. Sepúlveda-Escribano, J.L.G. Fierro, F. Rodríguez-Reinoso, Appl. Catal. A: General 150 (1997) 165.
[10] A.B. da Silva, E. Jordão, M.J. Mendes, P. Fouilloux, Appl. Catal. A: General 148 (1997) 253.
[11] M.A. Vannice, B. Sen, J. Catal. 115 (1989) 65.
[12] A. Giroir-Fendler, D. Richard, P. Gallezot, Heterogeneous catalysis and fine chemicals, in: M. Guisnet, J. Barrault, C. Bouchoule, D. Duprez, C. Montassier, G. Pérot (Eds.), Proceedings of the International Symposium, Poitiers, 15–17 March 1988, Stud. Surf. Sci. Catal., vol. 41, Elsevier, Amsterdam, 1988, p. 171.
[13] D.G. Blackmond, R. Oukaci, B. Blanc, P. Gallezot, J. Catal. 131 (1991) 401.
[14] M. Arai, K. Usui, Y. Nishiyama, J. Chem. Soc., Chem. Commun. 24 (1993) 1853.
[15] M. Arai, A. Obata, K. Usui, M. Shirai, Y. Nishiyama, Appl. Catal. A: General 146 (1996) 381.
[16] Z. Poltarzewski, S. Galvagno, R. Pietropaolo, P. Staiti, J. Catal. 102 (1986) 190.
[17] F. Coloma, A. Sepúlveda-Escribano, J.L.G. Fierro, F. Rodríguez-Reinoso, Appl. Catal. A: General 148 (1996) 63.
[18] S. Galvagno, A. Donato, G. Neri, R. Pietropaolo, G. Capannelli, J. Mol. Catal. 78 (1993) 227.
[19] G. Neri, L. Mercadante, C. Milone, R. Pietropaolo, S. Galvagno, J. Mol. Catal. A: Chemical 108 (1996) 41.
[20] G. Neri, C. Milone, A. Donato, L. Mercadante, A.M. Visco, J. Chem. Tech. Biotechnol. 60 (1994) 83.
[21] D.V. Sokokskii, N.V. Anisimova, A.K. Zharmagambetova, S.G. Mukhamedzhanova, L.N. Edygenova, React. Kinet. Catal. Lett. 33 (1987) 399.

[22] G. Gordier, French Patent F 2,329,628 (1975) to Rhône-Poulene S.A.
[23] E. Romeo, A.J. Marchi, A. Borgna, A. Monzón, in: A. Corma, F.V. Melo, S. Mendioroz, J.L.G. Fierro (Eds.), Proceedings of the 8th International Symposium on Catalyst Deactivation, Brugge, Belgium, 1999, Stud. Surf. Sci. Catal., vol. 126, Elsevier, Amsterdam, 1999, p. 113.
[24] R. Hubaut, M. Daage, J.P. Bonelle, Appl. Catal. 22 (1986) 231.
[25] R. Hubaut, J.P. Bonelle, M. Daage, J. Mol. Catal. 55 (1989) 170.
[26] H. Noller, J.E. German, J. Catal. 85 (1984) 25.
[27] T.R. Bonelle, R. Hubant, M. Daage, Appl. Catal. 22 (1986) 237.
[28] G.J. Hutchings, F. King, I.P. Okoye, C.H. Rochester, Catal. Lett. 23 (1994) 127.
[29] G.J. Hutchings, F. King, I.P. Okoye, C.H. Rochester, Appl. Catal. 83 (1992) L7.
[30] F. Trifirò, A. Vaccari, G. Braca, A.M. Raspolli Galletti, in: M.G. Scaros, M.L. Prunier (Eds.), Catalysis of Organic Reactions, Marcel Dekker, Inc., 1995, p. 475.
[31] P. Grandvallet, Ph. Courthy, E. Freund, in: Proceedings of the 8th International Congress on Catalysis, Berlin (West), 2–6 July 1984, DECHEMA, vol. II, 1984, p. 81.
[32] J.C. Rodríguez, A.J. Marchi, A. Borgna, A. Monzón, J. Catal. 171 (1997) 268.
[33] M.J.L. Ginés, A.J. Marchi, C.R. Apesteguía, Appl. Catal. A: General 154 (1997) 155.
[34] A.J. Marchi, J.I. Di Cosimo, C.R. Apesteguía, New frontiers in catalysis, in: L. Guczi, F. Solymosi, P. Tetenyi (Eds.), Proceedings of the 10th International Congress on Catalysis, 1992, vol. B, Elsevier, Amsterdam, 1993, p. 1771.
[35] A.J. Marchi, J.I. Di Cosimo, C.R. Apesteguía, Catalysis: theory to practice, C1 chemistry, in: M.J. Phillips, M. Ternan (Eds.), Proceedings of the 9th International Congress on Catalysis, Calgary, Alberta, Canada, 1988, vol. 2, The Chemical Institute of Canada, 1988, p. 529.
[36] A.J. Marchi, C.R. Apesteguía, Appl. Clay Sci. 13 (1998) 35.
[37] A.J. Marchi, J.L.G. Fierro, J. Santamaría, A. Monzón, Appl. Catal. 142 (1996) 375.
[38] B.R. Strohmeier, D.E. Leyden, R.S. Field, D.M. Hércules, J. Catal. 94 (1985) 514.
[39] A. Wolberg, J.F. Roth, J. Catal. 18 (1969) 250.
[40] P. Arnoldy, J.A. Moulijn, J. Catal. 93 (1985) 38.
[41] A.J. Marchi, J.I. Di Cosimo, C.R. Apesteguía, Catal. Today 15 (1992) 383.
[42] M.J.L. Ginés, C.R. Apesteguía, in: J.J. Spivey, E. Iglesia, T.H. Fleisch (Eds.), Stud. Surf. Sci. Catal., vol.136, Elsevier Science B.V., 2001, p. 447.
[43] K.H. Tonge, Thermochim. Acta 74 (1984) 151.
[44] R.A. Hadden, B. Sakakini, J. Tabatabaei, K.C. Waugh, Catal. Lett. 44 (1997) 145.
[45] P. Gallezot, D. Richard, Catal. Rev. Sci. Eng. 40 (1/2) (1998) 81.
[46] R. Rao, A. Dandekar, R.T.K. Baker, M.A. Vannice, J. Catal. 171 (1997) 406.
[47] A. Dandekar, R.T.H. Baker, M.A. Vannice, J. Catal. 184 (1999) 421.
[48] F. Delbecq, P. Sautet, J. Catal. 152 (1995) 217.
[49] M. Lashdaf, A.O.I. Krause, M. Lindblad, M. Tiitta, T. Venäläinen, Appl. Catal. A: General 241 (2003) 65.
[50] D. Richard, J. Ockelford, A. Giroir-Fendler, P. Gallezot, Catal. Lett. 3 (1989) 53.